Conventional superconductivity in quasicrystals

Ronaldo N. Araújo and Eric C. Andrade
Instituto de Física de São Carlos, Universidade de São Paulo, C.P. 369, São Carlos, SP, 13560-970, Brazil

(Received 28 March 2019; revised manuscript received 20 June 2019; published 11 July 2019)

Motivated by a recent experimental observation of superconductivity in the Al-Zn-Mg quasicrystal, we study the low-temperature behavior of electrons moving in the quasiperiodic potential of the Ammann–Beenker tiling in the presence of a local attraction. We employ the Bogoliubov–de Gennes approach for approximants of different sizes and determine the local pairing amplitude Δ_i as well its spatial average, Δ_0, the superconducting order parameter. Due to the lack of periodicity of the octagonal tiling, the resulting superconducting state is inhomogeneous, but we find no evidence of the superconductivity islands, as observed in disordered systems, with $\Delta_i \to 0$ at T_c for all sites. In the weak-coupling regime, we find that the superconducting order parameter depends appreciably on the approximant size only if the Fermi energy sits at a pseudogap in the noninteracting density of states, with Δ_0 decreasing as the system size increases. These results are in line with the experimental observations for the Al-Zn-Mg quasicrystal, and they suggest that, despite their electronic structure, quasicrystals are prone to display conventional BCS-like superconductivity.

DOI: 10.1103/PhysRevB.100.014510

I. INTRODUCTION

Quasicrystals display a nonperiodic, yet ordered, arrangement of atoms [1,2]. They contain a small set of local environments which reappear again and again, albeit not in a periodic fashion. Their structure is not random either, since the diffraction pattern shows sharp Bragg peaks, although their symmetry is noncrystallographic, with the n-fold symmetries ($n = 5, 8, 10, \ldots$) stemming from the fact that these local environments occur with n equiprobable orientations. Because of this arrangement of atoms, the Bloch theorem no longer holds and the electronic states of quasicrystals show a remarkably rich behavior [3,4], which includes critical states [5–9], confined states in the middle of the band [10–12], pseudogap in the density of states [13–16], and unconventional conduction properties [17–20].

Given their unusual electronic properties, there are several works addressing the effects of electronic correlations in quasicrystals, especially investigating their magnetic properties both in localized and itinerant regimes [21–25]. Although many interesting properties arise due to the intricate real-space arrangement of the lattice sites, some of the physical properties inside phases with long-range order are similar to those of periodic systems [26]. Therefore, the experimental observation of non-Fermi liquid behavior in the $Au_{51}Al_{34}Yb_{15}$ heavy-fermion quasicrystal [27] immediately prompted several theoretical studies [28–31].

Superconductivity was observed in approximants [32,33], which are periodic rational approximations to the quasicrystal, shortly after the discovery of quasicrystals. However, only recently a convincing observation of bulk superconductivity in the Al-Zn-Mg quasicrystal was reported [34]. Reference [34] finds that the critical temperature T_c is very low, $T_c \simeq 0.05$ K, and that T_c is suppressed as one goes from the approximants to the quasicrystal. Moreover, the authors show that the thermodynamic properties can be understood within the usual BCS weak-coupling scenario. Motivated by these experimental findings, in this paper we study the attractive Hubbard model in a bidimensional quasicrystal. We employ a Bogoliubov-de Gennes approach and our results provide a scenario which is consistent with the experimental observations.

Our paper is organized as follows. In Sec. II, we review the basic properties of the Ammann-Beenker tiling model and its electronic properties. In particular, we employ the Kohn's localization tensor to probe the spatial extent of the electronic states. In Sec. III, we introduce the attractive Hubbard model and the inhomogeneous Bogoliubov-de Gennes (BdG) mean-field theory to obtain the properties of our model inside the superconducting phase. In Sec. IV, we then compare our results to experiments and contrast our findings with the known results for random systems, after which we conclude the paper. We also have two appendices. Appendix A discusses the spectral function of the noninteracting model, while Appendix B introduces a complementary approach to study the superconductivity, namel,y the pairing of exact eigenstates (PoEE).

II. TILING MODEL AND ELECTRONIC PROPERTIES

For simplicity, we consider models on quasiperiodic tilings to mimic the geometrical properties of a quasicrystal. We report results obtained for a 2D tiling, where it is easier to handle large system sizes numerically [35]. The 2D tiling we consider is the octagonal, or Ammann-Beenker, tiling [36]. This tiling is composed of two types of decorated tiles: squares and 45° rhombuses, which combine to create six distinct local environments with coordination numbers $z = 3, \cdots, 8$, Fig. 1(a). These square approximants are obtained by the standard method of projecting down from a higher dimensional cubic lattice [36–39], and we consider approximant of sizes $N = 41$, 239, 1393, 8119, and 47321. Even though it is easy to convince oneself on the absence of translational

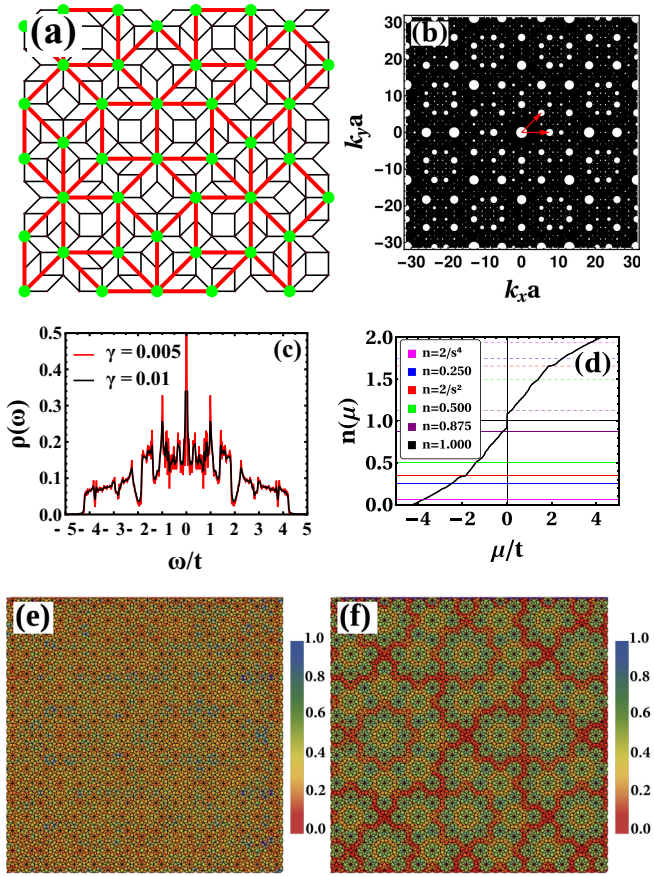

FIG. 1. (a) Square approximant for the perfect octagonal tiling with $N = 239$ sites. There are six local site environments with $z = 3, \ldots, 8$ nearest neighbors in the bulk. Nearest-neighboring sites are connected along the edges of the squares and the rhombuses. Superimposed inflated $N = 41$ approximant (thick lines) with its length rescaled by the silver ratio $s = 1 + \sqrt{2}$. (b) X-ray structure factor for the $N = 8119$ approximant displaying the underlying eightfold symmetry. The width of the disk indicates the intensity of the peak. The red arrows show the vectors $\pi s(1, 0)$ and $\pi s/\sqrt{2}(1, 1)$, connecting the Γ point to two of the neighboring brighter peaks. (c) Density of states for the $N = 47321$ approximant, calculated considering open boundary conditions and two broadening widths γ. (d) Integrated density of states showing the electronic filling as a function of the chemical potential. Local density of states for the $N = 8119$ approximant at the fillings: (e) $n = 0.25$ and (f) $n = 1.00$.

invariance by examining the real-space arrangement of the lattice sites in Fig. 1(a), the eightfold rotational symmetry (present at many different scales) becomes evident as we go to momentum space and calculate the x-ray structure factor, Fig. 1(b). The lack of periodicity manifests itself in reciprocal space both by the absence of a Brillouin zone and the presence of several intense Bragg peaks. As we increase the approximant size, more and more spots appear in the structure factor until it becomes densely filled in the reciprocal space in the limit of the infinite quasicrystal. Another important property of quasicrystals is their self-similarity under inflation transformations. These are site-decimation operations on a subset of vertices of the tiling followed by an increase in the length scale and the reconnection of the surviving vertices. It globally preserves the quasiperiodic structure, see Fig. 1(a), and the infinite quasicrystal is invariant under such transformation [38,40].

The presence of diffraction spots of widely differing intensities has important consequences on the electronic properties of the quasicrystal. In a periodic system, if the Fermi wave vector $\mathbf{k}_F$ satisfies $2\mathbf{k}_F = \mathbf{H}$, where $\mathbf{H}$ is a reciprocal lattice vector, a band gap is expected to emerge. In a quasicrystal, because the structure factor is densely filled, this condition is easily met and then we expect the brighter peaks to lead to strong scattering of conduction electrons, giving rise to spikes in the density of states (DOS) [see also Fig. 6(b)] [41,42]. The scattering due to the remaining peaks, while weaker, results in wave functions which show fluctuations at all length scales. The Fibonacci chain, a one-dimensional quasicrystal, provides an example of such wave functions [5], often referred to as *critical* [3–7,9], in analogy with those found at the Anderson metal-insulator transition [43–45].

As a minimal model to describe the electronic properties of quasicrystals, we study a nearest-neighbor tight-binding Hamiltonian in the Ammann-Beenker tiling,

$$\mathcal{H}_0 = -t \sum_{\langle ij\rangle,\sigma} (c^\dagger_{i\sigma} c_{j\sigma} + c^\dagger_{j\sigma} c_{i\sigma}), \tag{1}$$

where $c^\dagger_{i\sigma}(c_{i\sigma})$ is the creation (annihilation) operator of an electron at site i with spin σ and t is the hopping amplitude between sites i and j. In the following, energies are measured in units of t. In our calculation, we consider open boundary conditions because: (i) it preserves the particle-hole symmetry of the tiling and (ii) the finite size effects are comparable to those of periodic boundary conditions due to the quasiperiodic arrangement of the different local environments [24].

The resulting DOS $\rho(\omega) = (1/N)\sum_\nu \delta(\omega - \varepsilon_\nu)$, where ε_ν are the eigenenergies of $\mathcal{H}_0$ in Eq. (1), is shown in Fig. 1(c) (we replace each delta function by a Lorentzian of width γ). As anticipated, $\rho(\omega)$ displays a strong energy dependence with several spikes, which are largely independent of the broadening γ. The large peak at $\omega = 0$ can be traced to families of strictly localized states, a consequence of the local topology of the octagonal tiling [3,12]. The integrated density of states $n(\mu) = \int_{-\infty}^{\mu} d\omega \rho(\omega)$, μ is the chemical potential, is shown in Fig. 1(d). Besides the discontinuity close to $\mu = 0$, corresponding to the peak in $\rho(0)$, $n(\mu)$ also shows a kink at the filling $2/s^2 \approx 0.34315$, where $s = 1 + \sqrt{2}$ is the silver ratio. This is analogous to the case of the Fibonacci chain, where plateaus in $n(\mu)$ appear at $2/g^n$, where n is an integer and g is the golden ratio [8]. A plateau in $n(\mu)$ corresponds to a gap in the single-particle spectrum of Eq. (1). However, conversely to the one-dimensional case, the DOS in the Ammann-Beenker tiling has at most a pseudogap close to $\omega \approx -1.9t$, corresponding to the filling $2/s^2$, and thus we observe only a kink.

A pseudogap at the Fermi level assists in the stabilization of the quasiperiodic structure via the Hume–Rothery mechanism, and it is indeed predicted and observed in several quasicrystals [14,16,18,41,46–48].

The unambiguous existence of a pseudogap is hindered due to the finite broadening γ employed in the numerical calculation of $\rho(\omega)$. Therefore, we now probe the spatial

extent of the wave function, especially close to the filling $2/s^2$. First, we compute the inverse participation ratio (IPR),

$$\mathrm{IPR}_\nu = \sum_i |\psi_\nu(i)|^4, \tag{2}$$

where ψ_ν is an eigenstate of $\mathcal{H}_0$ with eigenenergy ε_ν. The scaling of the IPR with the system size is related to the spatial structure of the single-particle electronic states. If we write $\mathrm{IPR}_\nu \propto N^{-\beta}$, then $\beta = 1$ for extended and $\beta = 0$ for exponentially localized states. In a quasicrystal, we expect $0 \leqslant \beta \leqslant 1$, due to the multifractal character of the eigenstates [3,43,44,49]. In Fig. 2, we calculate IPR_ν at different positions in the band. For most fillings, we obtain $\beta \approx 0.90$, a value similar to the one observed in the Penrose tiling [3]. At the band center, we get $\beta \approx 1$, a value one expects for extended states (at half filling, we have flat bandlike structures coexisting with dispersive ones, see Appendix A). For $n = 2/s^2$, we have $\beta = 0.55(6)$. Although smaller than the values at the other fillings, this value does not indicate that this particular state is localized and it seems inconsistent with the presence of a pseudogap.

While the IPR is a very useful tool in the context of disordered systems, it may not be able to capture all the subtleties of quasicrystalline electronic states. Indeed, a recent study of the one-dimensional Fibonacci chain showed that the IPR is unable to capture the expected insulating behavior inside the band minigaps [50]. Following Ref. [50], we then decided to study the scaling behavior of the Kohn's localization tensor [51–53]:

$$\lambda_{\gamma\delta} = \frac{1}{N}\sum_{i,j}(\mathbf{r}_i - \mathbf{r}_j)_\gamma(\mathbf{r}_i - \mathbf{r}_j)_\delta |P(i,\ j)|^2. \tag{3}$$

Here $\mathbf{r}_i$ is the position of site i inside the approximant, γ, δ correspond to the spatial directions x and y, and $P(i,\ j) = \sum_\nu \psi_\nu(i)\psi_\nu^\star(j)$, with $\varepsilon_\nu \leqslant \mu$, is the one-particle density matrix for a Slater determinant. Therefore, the localization tensor takes into account all states up to the chemical potential and not only a single-particle state. Because time-reversal symmetry is preserved in the problem, the transverse terms vanish identically: $\lambda_{xy} = \lambda_{yx} = 0$. Moreover, we have $\lambda_{xx} = \lambda_{yy} = \lambda$, so we drop the spatial subscripts henceforth. The scaling of length λ with the approximant size then determines if the system is a metal or an insulator. In a metal, we expect λ^2 to diverge with N, whereas for an insulator we expect λ^2 to saturate to a constant [50]. If we write $\lambda^{-2} \propto N^{-\alpha}$, we then expect $0 \leqslant \alpha \leqslant 1$. The results for the scaling of Kohn's localization tensor are displayed in Fig. 2(b), where it is clear that its dependence with the band filling is indeed more pronounced as compared to the IPR. For arbitrary filling, the states have an extendedlike nature, particularly at the band center where we have $\alpha \approx 1$. For the filling $n = 2/s^2$, however, λ^{-2} is weakly size dependent, $\alpha \approx 0.1$, suggesting a localizedlike nature for this state, consistent with the presence of a pseudogap.

Overall, we find that the Kohn's localization tensor has a stronger dependence with the band filling and it is better suited to decide whether the electronic states are conducting or insulating [50]. We stress, however, that λ is not simply related to the spatial extent of the single-particle eigenstates, and a more detailed characterization of the multifractal character of the eigenstates is not straightforward within this formalism.

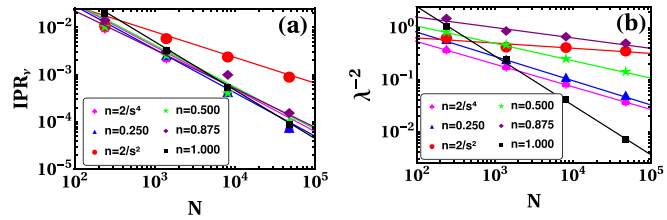

FIG. 2. (a) Inverse participation ratio IPR_ν as a function of the approximant size N for different fillings n on a log-log plot. We fit $\mathrm{IPR}_\nu \propto N^{-\beta}$. (b) Same as (a) for the Kohn's localization tensor. We fit $\lambda^{-2} \propto N^{-\alpha}$.

III. SUPERCONDUCTIVITY

After discussing the electronic properties of the octagonal tiling, we now move to the main topic of this paper, which is the study of superconductivity. We describe an s-wave superconductor using the attractive Hubbard Hamiltonian,

$$\mathcal{H} = \mathcal{H}_0 - U\sum_i n_{i\uparrow}n_{i\downarrow}, \tag{4}$$

where $\mathcal{H}_0$ is given by Eq. (1), $U > 0$ is the uniform on-site pairing attraction, and $n_{i\sigma} = c_{i\sigma}^\dagger c_{i\sigma}$ is the number operator. This model naturally neglects the effects of Coulomb interaction, as well as the nontrivial phonon spectrum of quasicrystals [54–58]. However, we feel that it is a useful exercise to understand the physics of this simple model, where we can contrast our results with a similar investigation in the Penrose tiling [59]. Moreover, we will show that it provides a useful starting point to understand the recently reported quasicrystal superconductivity [34].

We study the model in Eq. (4) for different values of the pairing attraction U and filling n. Because the DOS in a quasicrystal is strongly energy dependent, Fig. 1(c), one could expect, in principle, strong filling dependence of the results. Nevertheless, as we discussed in the previous section, the behavior of the electronic states is qualitatively the same for all fillings, i.e., metalliclike, except at the special filling of $2/s^2$ where we observe an insulating behavior due to a pseudogap in the DOS.

To solve the Hamiltonian Eq. (4), we employ the BdG approach, following the works in Refs. [60,61], to write the mean-field Hamiltonian:

$$\mathcal{H}_{\mathrm{BdG}} = -t\sum_{\langle ij\rangle,\sigma}(c_{i\sigma}^\dagger c_{j\sigma} + c_{j\sigma}^\dagger c_{i\sigma}) - \sum_{i,\sigma}\tilde{\mu}_i n_{i\sigma} + \sum_i(\Delta_i c_{i\uparrow}^\dagger c_{i\downarrow}^\dagger + \Delta_i^\star c_{i\downarrow}c_{i\uparrow}). \tag{5}$$

The local pairing amplitude Δ_i and the local density n_i are determined via the self-consistent equations,

$$\Delta_i = -U\langle c_{i\downarrow}c_{i\uparrow}\rangle, \quad \langle n_i\rangle = \sum_\sigma\langle c_{i\sigma}^\dagger c_{i\sigma}\rangle, \tag{6}$$

where the thermal averages are taken considering the eigenstates and eigenenergies of Eq. (5), which we determine via

a numerical Bogoliubov transformation. We also introduce an effective chemical potential to incorporate a site-depend Hartree shift: $\tilde{\mu}_i = \mu + U\langle n_i\rangle/2$, building thus the most general mean-field theory for an inhomogeneous s-wave superconductor [62]. We remark that this mean-field theory keeps only the amplitude fluctuations of Δ_i and should only be valid at weak coupling.

We solve the self-consistency Eqs. (6) on finite approximants with N sites, open boundary conditions, and fixed electronic filling $n = \sum_i n_i/N$. We consider $U \geqslant 1.5t$ because smaller values of U generate very large coherence lengths and are harder to simulate. To solve Eqs. (6), we start with an initial guess for the local density n_i and the pairing amplitude Δ_i, and we iterate the procedure until convergence is achieved on all sites. We then adjust the chemical potential μ to target the desired filling n. Notice, therefore, that we have two self-consistency loops, making the whole procedure quite demanding numerically. To complement this procedure, and to access larger system sizes, we also implement the method of PoEE [60,61] (see Appendix B).

We start by showing the spatial distribution of the local pairing amplitude Δ_i at $T = 0$ in Figs. 3(a) and 3(b). For small values of the pairing attraction U, the spatial pattern of Δ_i roughly follows that of the local density of states [63], see Figs. 1(e) and 1(f), and it is essentially determined by the local environment of a given site i. At low fillings, the sites with a larger coordination number z show larger values of Δ_i, whereas for $n \to 1$ sites with smaller z are the ones with larger Δ_i, Figs. 3(c) and 3(d). Importantly, we do not observe the formation of superconducting islands as in disordered superconductors [60,61,64–67]. This is not unexpected because these islands occur in regions where the random disorder potential is unusually small, corresponding thus to rare regions [68,69], a situation which cannot take place in the presence of a deterministic quasiperiodic potential obeying inflation rules. Because the distribution of Δ_i consists essentially of six delta peaks, each one associated to a local environment, and is neither broad nor shows weight at $\Delta_i \approx 0$, we also conclude that the system is far away from a possible quasiperiodicity-induced quantum phase transition.

In smaller approximants, $N \leqslant 1393$, we are able to solve the BdG solutions at finite temperatures, Figs. 3(e) and 3(f). Even though Δ_i is spatially inhomogeneous, we find that the superconducting phase transition takes place at all approximant sites at once within our numerical precision. In a translational invariant system, we naturally expect all Δ_i's to vanish concomitantly at T_c. For the octagonal tiling, we believe that its self-similarity under inflation transformations, see Fig. 1(a), forces all Δ_i's to vanish simultaneously at T_c. To see this, suppose we start with a subset of sites for which $\Delta_i = 0$ inside the superconducting phase. Now we successively apply the inflation transformations (remember also that Δ_i is essentially determined by its local environment). Because these transformations leave the infinite system invariant due to their self-similarity, we would then be able to eventually move the entire system to the normal phase. This argument also highlights that the existence of rare regions is not possible, thus precluding both the existence of the superconducting islands at $T = 0$, as discussed before, and the presence of a thermal Griffiths phase close to T_c.

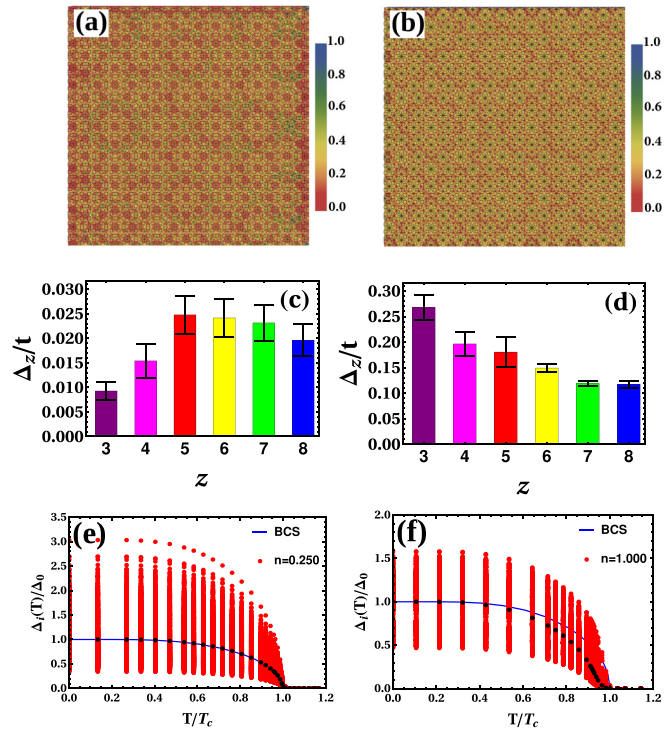

FIG. 3. Color plots of local pairing amplitude Δ_i, normalized by its maximum value: (a) $n = 0.25$ and (b) $n = 1.00$. Average value of the local pairing amplitude for a given local environment characterized by the coordination number z, Δ_z. The height of the bars give the average value and the black lines the standard deviation: (c) $n = 0.25$ and (d) $n = 1.00$. Here we considered $T = 0$, the approximant with $N = 8119$ sites, and $U = 1.5t$. Temperature dependence, rescaled by T_c, of the the local pairing amplitude Δ_i, divided by Δ_0, for the $N = 1393$ approximant and two different fillings: (e) $n = 0.25$ [$T_c/t = 0.011$, $\Delta_0 = 0.015(6)$] and (f) $n = 1.00$ [$(T_c/t = 0.13$, $\Delta_0 = 0.22(5)$]. We compare the results with BCS theory (blue curve). The black dots represent the average value of Δ_i, whereas the red dots show all values of Δ_i for the tiling.

To explore the role of the coherence length ξ—as defined by the spatial decay of the sample averaged correlation function $\langle\Delta_i\Delta_j\rangle$—we study the Fourier transform of both Δ_i and n_i, see Fig. 4. The Fourier transform of Δ_i shows the expected eightfold structure, as in Fig. 1(b), but there are several missing peaks which we link to the presence of a coherence length ξ (ξ is the largest, circa 10 lattice spacing, at the pseudogap $n = 2/s^2$). As we increase the local attraction U, the Cooper pairs become more and more local, resulting in the suppression of ξ and in the observation of a densely filled Δ_i spectrum in reciprocal space. The local density n_i, on the other hand, is quite insensitive to U as it varies on the scale of one lattice spacing, always following the lattice potential.

We now investigate the superconducting ground-state evolution as a function of the approximant size N. On one hand—based on previous studies considering the multifractal states observed at the Anderson metal-insulator transition—[43–45] one could naively expect an enhancement of the superconductivity [70,71] as one moves toward the infinite quasicrystal since the electronic states become more and more critical. On the other hand, all experiments so far find a

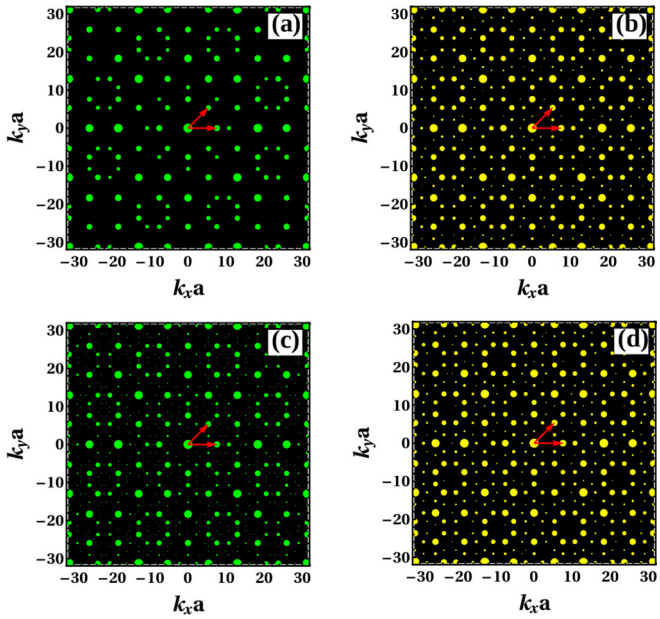

FIG. 4. Fourier transform of the local pairing amplitude, (a) and (c), and the local electronic density n_i, (b) and (d), for $n = 2/s^2$ with $U = 1.5t$, (a) and (b), and $U = 6.0t$, (c) and (d). The width of the disk indicates the intensity of the peak. The red arrows are the same as in Fig. 1(b). Here we considered $N = 8119$.

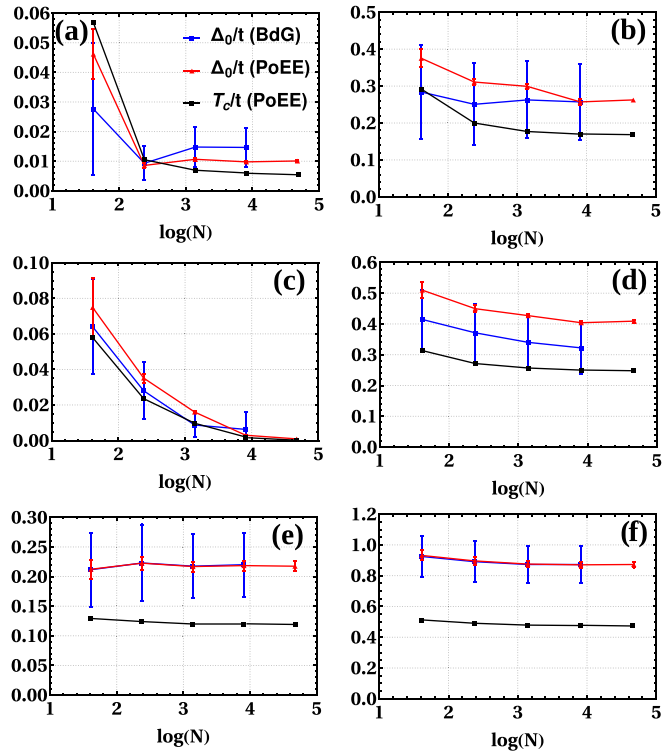

FIG. 5. Superconducting order parameter $\Delta_0 = \sum_i \Delta_i/N$ and critical temperature T_c as a function of the approximant size N. We show the results from both the Bogoliubov-de Gennes (BdG) (Δ_0) and the pairing of exact eigenstates (PoEE) (Δ_0, T_c) methods. (a) $U = 1.5t$ and $n = 0.25$; (b) $U = 3.0t$ and $n = 0.25$; (c) $U = 1.5t$ and $n = 2/s^2$; (d) $U = 3.0t$ and $n = 2/s^2$; (e) $U = 1.5t$ and $n = 1.00$; (f) $U = 3.0t$ and $n = 1.00$.

reduction, or even a complete suppression, of T_c as one goes from the approximant to the quasicrystal [32–34]. In Fig. 5, we show the superconducting order parameter $\Delta_0 = \sum_i \Delta_i/N$ and T_c as a function of the approximant size N. We compare the results for Δ_0 using the full numerical solution of the BdG equations, Eqs. (6), and that coming from the PoEE, Eqs. (B3) and (B4) [the PoEE is cheaper numerically and allows us to go up to $N = 47321$ and also to estimate T_c, see Eq. (B5)]. We find that Δ_0 and T_c remain essentially constant for $N \geqslant 239$ at all fillings but $n = 2/s^2$, and the results of both methods agree even quantitatively. This implies that the approximants are able to capture the behavior of the infinite quasicrystal, and that the nature of the electronic wave functions in the infinite quasicrystal does not affect its superconductivity. This somewhat disappointing result also shows that the expected analogy to disordered systems close to the Anderson metal-insulator transition does not hold (for all parameter sets we simulate, considering $U \geqslant 1.5t$, we find no enhancement superconductivity as we increase N). Our scaling results for a general filling in Fig. 5 also do not agree with the experimentally observed suppression of T_c as N increases. The only filling which captures the experimental trend is $n = 2/s^2$, corresponding to the pseudogap in the DOS. Here, both Δ_0 and T_c are suppressed, at weak coupling, as we increase the approximant size, due to the pseudogap in the DOS. From Fig. 2(b), we see that the pseudogap gets more and more pronounced as N increases, and for $N \to \infty$ we must have $U > U_c$, a critical coupling, for the system to display superconductivity. For $U = 1.5t$, the PoEE approach suggests that $\Delta_0 \to 0$, whereas the full BdG solution finds $\Delta_0 > 0$, albeit small. The difference comes from the fact that the BdG method modifies the eigenstates of the noninteracting Hamiltonian, and it shows that we are already above the critical coupling U_c. As U increases, all fillings behave similarly and the results are essentially size independent. Therefore, the suppression of T_c in a quasicrystal occurs only if the Fermi level sits at a pseudogap—a condition routinely met in real quasicrystals—and at weak coupling.

IV. DISCUSSION AND CONNECTION TO EXPERIMENTS

Our results show that the physics observed at the mean-field level in randomly disordered superconductors is not present in quasicrystals. In particular, we do not observe the formation of superconducting islands due to the deterministic character of the lattice potential we consider [38], a conclusion which should be valid for a broad range of quasicrystals that can be similarly constructed via inflation or substitution rules. As was recently shown [67], the existence of such islands circumvents Anderson's theorem [72,73] and generically enhances T_c. We also do not find an increase of T_c due to the multifractal nature of the electronic state in the infinite quasicrystal, as is expected for disordered systems close to the Anderson metal-insulator transition [70,71]. Taken together, these observations imply that the BdG solution for superconductivity in a quasicrystal essentially fulfills Anderson's theorem, i.e. the electrons form pairs with time-reversed eigenstates, say $\nu \uparrow$ and $\bar{\nu} \downarrow$, of the noninteracting model. Thus the superconductivity is of the conventional weak-coupling BCS type, with both T_c and Δ_0 depending

weakly on N (this point is further supported by the excellent agreement between the results of the BdG and PoEE methods in Fig. 5). An interesting consequence of this observation is the fact that Anderson's theorem also implies that T_c does not depend on the wave functions of $\mathcal{H}_0$, but only on its spectrum, and thus T_c should be mainly governed by the DOS in Fig. 1(c). Our scaling of the order parameter Δ_0 in Fig. 5 illustrates this conclusion as the only distinct behavior is observed at the pseudogap and at weak-coupling. Concerning the finite temperature critical properties of the model, the absence of rare regions, together with the fact that Luck's criterion [26] holds for the octagonal tilling (as it does for most tilings constructed via inflation rules), implies that the mean-field BCS solution is expected to hold, as is observed experimentally [34].

Although the filling $n = 2/s^2$ looks like a finely tuned exception in our model, this point is actually very relevant experimentally, since in most quasicrystals the Fermi energy is located at a pseudogap [13–16]. Because of that, our results naturally account for the suppression of superconductivity as one goes from the approximant to the quasicrystal [32,33], and for the conventional superconductivity in the Al-Zn-Mg quasicrystal, as reported in Ref. [34]. One obvious implication of our findings is that a small amount of nonmagnetic impurities should enhance T_c in a quasicrystal, similarly to what is predicted for superconducting semimetals [65–67]. A similar possibility to increase T_c is to dope the system, moving the Fermi level away from the pseudogap.

We can also use our results to understand the absence of superconductivity in $Au_{51}Al_{34}Yb_{15}$ [27] and other related heavy-fermion quasicrystals [33]. In this class of quasicrystals, a non-Fermi liquid behavior was reported without the tuning of an external parameter [27]. Interestingly, such electronic behavior is absent in the approximants. A plausible scenario to understand these observations is the presence of unscreened magnetic moments down to $T \to 0$ in the quasicrystals, while in the approximants the moments are always screened below a temperature $T^\star$ [30]. Therefore, while superconductivity is observed in the approximants of heavy-fermion quasicrystals [33], the unscreened local moments in quasicrystals act as local pair-breaking defects and further suppress the superconductivity, making it unlikely for this phase to appear in an experimentally accessible temperature.

Overall, despite the fractal geometry of quasicrystals [74], the observation of unconventional superconductivity in quasicrystals [59] will probably require the same ingredients as in periodic metals, meaning appreciable electron-electron interaction, most likely in a material which does not involve f electrons. Another interesting problem would be to understand the compounds with a strong electron-phonon coupling where the ubiquitous phonon spectrum of quasicrystals would come into play [58], contrasting these findings with superconductivity in elastically strained crystals where the electronic structure is modulated in response to local lattice deformations [75].

V. CONCLUSIONS

In this paper, we have studied the electronic properties and the s-wave superconductivity in the two-dimensional Ammann-Beenker tiling. For the electronic properties, we employed the Kohn's localization tensor and the IPR to access the extent of the electronic states. As in one-dimensional examples [50], we find that the localization tensor gives a more detailed account on the conduction properties of a quasiperiodic system, as shown, for instance, in the better description of the insulating behavior expected for the pseudogap at $n = 2/s^2$.

To investigate the superconductivity, we considered both real-space BdG and the PoEE approaches to calculate the local pairing amplitude Δ_i. We show that Δ_i is essentially determined by its local environment and that the formation of superconducting islands is absent due to the deterministic nature of the lattice potential we consider [38]. Therefore, we find conventional BCS superconductivity in a quasicrystal, despite the nature of their noninteracting electronic states. The pairing mechanism is the one suggested by Anderson [72], with time-reversed eigenstates forming the Cooper pairs. In the weak-coupling limit, the superconductivity is suppressed at the pseudogap as we increase the approximant size. Our findings are in accordance with recent experimental observations [34].

Since the physics of rare events, which has profound effects in random inhomogeneous systems [76], is absent in quasicrystals, one may expect their electronic and magnetic responses to display a more conventional behavior whenever long-range order is present [21–24,77]. Of course, the local response is still highly nontrivial due to the fractal geometry of quasicrystalline lattice [27,30], and future work on correlation effects on quasicrystals are certain to provide many more surprises, an avenue that nowadays can also be explored using different platforms such as cold atoms [78], electronic systems with incommensurate order [79], or strongly correlated electronic systems at fractional filling [80].

ACKNOWLEDGMENTS

We acknowledge J. H. Garcia, J. A. Hoyos, G. F. Magno, P. B. Mendonça, and R. T. Scalettar for useful discussions. R.N.A was supported by the CAPES (BR)—Finance Code 001. E.C.A. was supported by CNPq (BR) Grant No. 302065/2016-4.

APPENDIX A: SPECTRAL FUNCTION

To gain further insight on the electronic structure of the noninteracting model, we calculate the spectral function

$$A(\boldsymbol{k}, \omega) = \sum_{\nu} \delta(\omega - \varepsilon_\nu)|\psi_\nu(\boldsymbol{k})|^2, \tag{A1}$$

where $\psi_\nu(\boldsymbol{k})$ is the νth eigenstate of the noninteracting tight-binding Hamiltonian $\mathcal{H}_0$, projected onto the momentum basis, and ε_ν is its corresponding eigenenergy. To calculate $A(\boldsymbol{k}, \omega)$ numerically, we represent the Dirac-delta function as a Lorentzian with a broadening $\gamma = 0.01t$.

In Fig. 6(a), we show the constant energy surfaces for the filling $2/s^2$ and the eightfold rotation symmetry is evident [47,48]. Because of the pseudogap, the Fermi-surface-like contours are broken into pockets which are centered around the brightest x-ray spots displayed in Fig. 1(b). Since we have a dense set of Bragg peaks, there are several of these

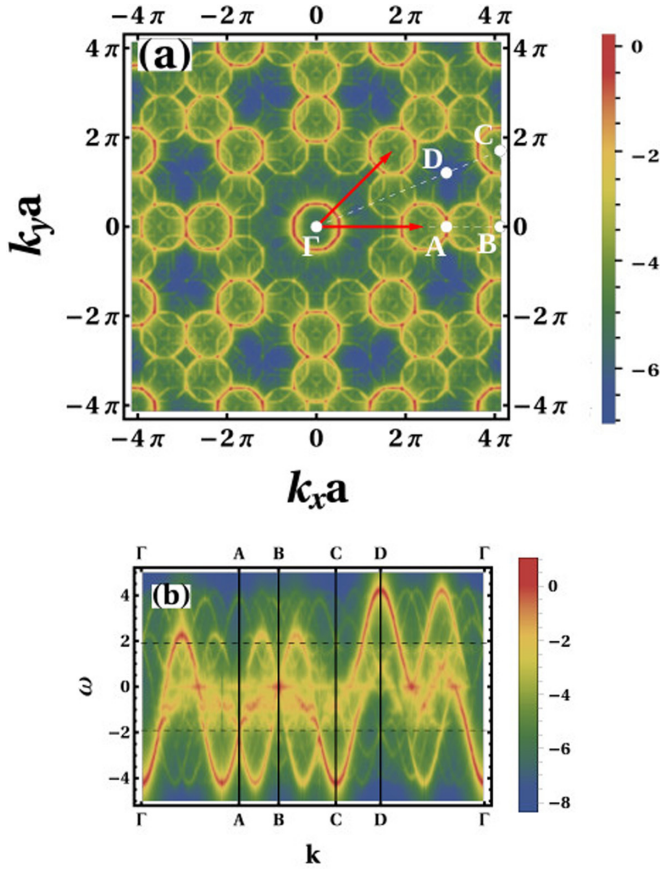

FIG. 6. (a) Surfaces of constant energy for the filling $n = 2/s^2$. The color intensity is determined by the spectral function $A(\boldsymbol{k}, \omega)$ and is shown in a log scale. The vectors shown here are the ones in Fig. 1(b) connecting the brightest Bragg peaks. (b) Energy as a function of momentum for the path defined in (a). The dashed lines set the energy of the pseudogap. Again, the color intensity is determined by the spectral function $A(\boldsymbol{k}, \omega)$ and is shown in a log scale. These results were obtained for the approximant with $N = 8119$ sites.

pockets and they intersect each other, making an immediate association to a pseudogap difficult in a finite approximant, where we superimpose our numerical broadening to the true physical broadening of the curves, coming from the fact that momentum is not a good quantum number (see the finite size scaling in Fig. 2).

The energy as a function of momentum, for a given path in reciprocal space, is displayed in Fig. 6(b). There, we see that close to the band edges the dispersionlike curves show a parabolic behavior. Therefore, a nearly-free-electron viewpoint appears to be a good starting point to understand the electronic properties of quasicrystals at these extreme fillings [41]. As we move on toward the band center, the dispersive features become more and more blurred due to the presence of gap openings at the crossing of the many parabolic bandlike curves. The boundaries between these two regimes are roughly set by the location of the pseudogap, where seemly linearly dispersing features are present [19]. Precisely at the band center, there is a flat bandlike structure, which can be directly linked to the huge peak in the DOS in Fig. 1(c). However, one also observes dispersive features, confirming that at half filling, the model given by Eq. (1) is metallic.

APPENDIX B: PAIRING OF EXACT EIGENSTATES (PoEE)

To complement the BdG results in the main text, we also consider the so-called pairing of exact eigenstates [60,61]. This approach is a generalization of Anderson's original idea of pairing an exact eigenstate of an inhomogeneous system to its time-reversed pair [72]. Since this formalism considers only the eigenstates and eigenenergies of Eq. (1), it allows us to investigate up to the $N = 47321$ approximant. A full self-consistent solution of the BdG equations for this number of sites is computationally prohibitive within our exact diagonalization scheme, although it may be possible using, for example, the kernel polynomial method [81,82].

We now briefly review the method. We start with the eigenstates ψ_ν of the noninteracting Hamiltonian $\mathcal{H}_0$ in Eq. (1). We then pair up electrons in time-reversed eigenstates, say $\nu\uparrow$ and $\bar{\nu}\downarrow$. The analogous BCS Hamiltonian in this basis is then given by [83]

$$\tilde{\mathcal{H}} = \sum_{\nu,\sigma} \xi_\nu c^\dagger_{\nu\sigma} c_{\nu\sigma} - U \sum_{\nu,\zeta} M_{\nu,\zeta} c^\dagger_{\nu\uparrow} c^\dagger_{\bar{\nu}\downarrow} c_{\bar{\zeta}\downarrow} c_{\zeta\uparrow}, \tag{B1}$$

where the matrix $M_{\nu,\zeta}$ is given by

$$M_{\nu,\zeta} = \sum_i |\psi_\nu(i)|^2 |\psi_\zeta(i)|^2, \tag{B2}$$

and $\xi_\nu = \varepsilon_\nu - \tilde{\mu}$ is the energy of the noninteracting problem measured with respect to effective, Hartree-shifted, chemical potential. A mean-field treatment of Eq. (B1) then leads to the following set of self-consistent equations:

$$\Delta_\nu = U \sum_\zeta M_{\nu,\zeta} \frac{\Delta_\zeta}{2E_\zeta} \tanh \frac{E_\zeta}{2T}, \tag{B3}$$

$$\langle n \rangle = \frac{1}{N} \sum_\nu \left(1 - \frac{\xi_\nu}{E_\nu} \tanh \frac{E_\nu}{2T} \right), \tag{B4}$$

where $E_\nu = \sqrt{\xi_\nu^2 + \Delta_\nu^2}$ and T is the temperature. The first equation determines the pairing amplitude of each eigenstate ν, whereas the second one fixes the effective chemical potential $\tilde{\mu}$ (notice here we are only able to fix the average electronic density in the system). Once we solve these equations, we can then obtain the real space pairing amplitudes at $T = 0$ [60,61], and we have that $\langle \Delta_i \rangle = \langle \Delta_\nu \rangle = \Delta_0$. The scaling of the order parameter is shown in Fig. 5 and we see that the PoEE results nicely follow the full BdG solution, thus confirming Anderson's pairing and pointing to the conventional nature of the superconductivity in quasicrystals.

If we now linearize Eq. (B3), we get the following set of linear equations:

$$\Delta_\nu = \sum_\zeta B_{\nu\zeta}(T) \Delta_\zeta, \tag{B5}$$

where we defined the matrix $B_{\nu,\zeta}(T) = U M_{\nu,\zeta} \tanh(|\xi_\zeta|/2T)/|\xi_\zeta|$. T_c is then given by temperature where the largest eigenvalue of $B_{\nu,\zeta}(T)$ becomes equal to 1 with $\langle n \rangle$ fixed [although $B_{\nu,\zeta}(T)$ is nonsymmetric, we

checked that its eigenvalues are real]. The resulting T_c are also shown in Fig. 5, and we can compare it with the BdG results for $N = 1393$ in Figs. 3(c) and 3(d). For $n = 0.25$, we have $T_c/t = 0.011$ (BdG) and 0.008 (PoEE) whereas for $n = 1.00$ we have $T_c/t = 0.137$ (BdG) and 0.120 (PoEE), again showing a good agreement between the methods.

[1] D. Shechtman, I. Blech, D. Gratias, and J. W. Cahn, Metallic Phase with Long-Range Orientational Order and no Translational Symmetry, Phys. Rev. Lett. **53**, 1951 (1984).

[2] D. Levine and P. J. Steinhardt, Quasicrystals: A New Class of Ordered Structures, Phys. Rev. Lett. **53**, 2477 (1984).

[3] U. Grimm and M. Schreiber, Energy spectra and eigenstates of quasiperiodic tight-binding Hamiltonians, in *Quasicrystals—Structure and Physical Properties*, edited by H.-R. Trebin (Wiley-VCH, Weinheim, 2003).

[4] A. Jagannathan and F. Piéchon, Energy levels and their correlations in quasicrystals, Philos. Mag. **87**, 2389 (2007).

[5] M. Kohmoto, B. Sutherland, and C. Tang, Critical wave functions and a Cantor-set spectrum of a one-dimensional quasicrystal model, Phys. Rev. B **35**, 1020 (1987).

[6] H. Tsunetsugu, T. Fujiwara, K. Ueda, and T. Tokihiro, Electronic properties of the Penrose lattice. I. Energy spectrum and wave functions, Phys. Rev. B **43**, 8879 (1991).

[7] H. Q. Yuan, U. Grimm, P. Repetowicz, and M. Schreiber, Energy spectra, wave functions, and quantum diffusion for quasiperiodic systems, Phys. Rev. B **62**, 15569 (2000).

[8] D. Tanese, E. Gurevich, F. Baboux, T. Jacqmin, A. Lemaître, E. Galopin, I. Sagnes, A. Amo, J. Bloch, and E. Akkermans, Fractal Energy Spectrum of a Polariton Gas in a Fibonacci Quasiperiodic Potential, Phys. Rev. Lett. **112**, 146404 (2014).

[9] N. Macé, A. Jagannathan, P. Kalugin, R. Mosseri, and F. Piéchon, Critical eigenstates and their properties in one- and two-dimensional quasicrystals, Phys. Rev. B **96**, 045138 (2017).

[10] M. Kohmoto and B. Sutherland, Electronic States on a Penrose Lattice, Phys. Rev. Lett. **56**, 2740 (1986).

[11] M. Arai, T. Tokihiro, T. Fujiwara, and M. Kohmoto, Strictly localized states on a two-dimensional Penrose lattice, Phys. Rev. B **38**, 1621 (1988).

[12] T. Rieth and M. Schreiber, Identification of spatially confined states in two-dimensional quasiperiodic lattices, Phys. Rev. B **51**, 15827 (1995).

[13] T. Fujiwara, Electronic structure in the Al-Mn alloy crystalline analog of quasicrystals, Phys. Rev. B **40**, 942 (1989).

[14] T. Fujiwara and T. Yokokawa, Universal Pseudogap at Fermi Energy in Quasicrystals, Phys. Rev. Lett. **66**, 333 (1991).

[15] A. Ishikawa, Y. Takagiwa, K. Kimura, and R. Tamura, Probing of the pseudogap via thermoelectric properties in the Au-Al-Gd quasicrystal approximant, Phys. Rev. B **95**, 104201 (2017).

[16] S. Jazbec, S. Vrtnik, Z. Jagliččić, S. Kashimoto, J. Ivkov, P. Popcčević, A. Smontara, Hae Jin Kim, Jin Gyu Kim, and J. Dolinsăek, Electronic density of states and metastability of icosahedral Au-Al-Yb quasicrystal, J. Alloys Compd. **586**, 343 (2014).

[17] F. S. Pierce, S. J. Poon, and Q. Guo, Electron localization in metallic quasicrystals, Science **261**, 737 (1993).

[18] G. Trambly de Laissardière and T. Fujiwara, Electronic structure and transport in a model approximant of the decagonal quasicrystal Al-Cu-Co, Phys. Rev. B **50**, 9843 (1994).

[19] T. Timusk, J. P. Carbotte, C. C. Homes, D. N. Basov, and S. G. Sharapov, Three-dimensional Dirac fermions in quasicrystals as seen via optical conductivity, Phys. Rev. B **87**, 235121 (2013).

[20] G. T. de Laissardière and D. Mayou, Anomalous electronic transport in quasicrystals and related complex metallic alloys, C. R. Phys. **15**, 70 (2014).

[21] S. Wessel, A. Jagannathan, and S. Haas, Quantum Antiferromagnetism in Quasicrystals, Phys. Rev. Lett. **90**, 177205 (2003).

[22] A. P. Vieira, Low-Energy Properties of Aperiodic Quantum Spin Chains, Phys. Rev. Lett. **94**, 077201 (2005).

[23] S. Thiem and J. T. Chalker, Long-range magnetic order in models for rare-earth quasicrystals, Phys. Rev. B **92**, 224409 (2015).

[24] N. Hartman, W.-T. Chiu, and R. T. Scalettar, Magnetic correlations in a periodic Anderson model with nonuniform conduction electron coordination, Phys. Rev. B **93**, 235143 (2016).

[25] A. Koga and H. Tsunetsugu, Antiferromagnetic order in the Hubbard model on the Penrose lattice, Phys. Rev. B **96**, 214402 (2017).

[26] J. M. Luck, A classification of critical phenomena on quasicrystals and other aperiodic structures, Europhys. Lett. **24**, 359 (1993).

[27] K. Deguchi, S. Matsukawa, N. K. Sato, T. Hattori, K. Ishida, H. Takakura, and T. Ishimasa, Quantum critical state in a magnetic quasicrystal, Nat. Mater. **11**, 1013 (2012).

[28] S. Watanabe and K. Miyake, Robustness of quantum criticality of valence fluctuations, J. Phys. Soc. Jpn. **82**, 083704 (2013).

[29] V. R. Shaginyan, A. Z. Msezane, K. G. Popov, G. S. Japaridze, and V. A. Khodel, Common quantum phase transition in quasicrystals and heavy-fermion metals, Phys. Rev. B **87**, 245122 (2013).

[30] E. C. Andrade, A. Jagannathan, E. Miranda, M. Vojta, and V. Dobrosavljević, Non-Fermi-Liquid Behavior in Metallic Quasicrystals with Local Magnetic Moments, Phys. Rev. Lett. **115**, 036403 (2015).

[31] S. Takemura, N. Takemori, and A. Koga, Valence fluctuations and electric reconstruction in the extended Anderson model on the two-dimensional Penrose lattice, Phys. Rev. B **91**, 165114 (2015).

[32] J. E. Graebner and H. S. Chen, Specific Heat of an Icosahedral Superconductor, $Mg_3Zn_3Al_2$, Phys. Rev. Lett. **58**, 1945 (1987).

[33] K. Deguchi, M. Nakayama, S. Matsukawa, K. Imura, K. Tanaka, T. Ishimasa, and N. K. Sato, Superconductivity of Au-Ge-Yb approximants with Tsai-type clusters, J. Phys. Soc. Jpn. **84**, 023705 (2015).

[34] K. Kamiya, T. Takeuchi, N. Kabeya, N. Wada, T. Ishimasa, A. Ochiai, K. Deguchi, K. Imura, and N. K. Sato, Discovery of superconductivity in quasicrystal, Nat. Commun. **9**, 154 (2018).

[35] As argued in Ref. [54], the lower critical dimension for the existence of critical states in quasicrystals is 1D. In this sense, there should not be significant qualitative differences between electronic quasicrystalline states in 2D and 3D.

[36] J. E. S. Socolar, Simple octagonal and dodecagonal quasicrystals, Phys. Rev. B **39**, 10519 (1989).

[37] D. Levine and P. J. Steinhardt, *The Physics of Quasicrystals* (World Scientific, Singapore, 1987).

[38] M. Duneau, R. Mosseri, and C. Oguey, Approximants of quasiperiodic structures generated by the inflation mapping, J. Phys. A: Math. Gen. **22**, 4549 (1989).

[39] V. G. Benza and C. Sire, Band spectrum of the octagonal quasicrystal: Finite measure, gaps, and chaos, Phys. Rev. B **44**, 10343 (1991).

[40] A. Jagannathan, Self-similarity under inflation and level statistics: A study in two dimensions, Phys. Rev. B **61**, R834 (2000).

[41] A. P. Smith and N. W. Ashcroft, Pseudopotentials and Quasicrystals, Phys. Rev. Lett. **59**, 1365 (1987).

[42] E. S. Zijlstra and T. Janssen, Non-spiky density of states of an icosahedral quasicrystal, Europhys. Lett. **52**, 578 (2000).

[43] A. Richardella, P. Roushan, S. Mack, B. Zhou, D. A. Huse, D. D. Awschalom, and A. Yazdani, Visualizing critical correlations near the metal-insulator transition in $Ga_{1-x}Mn_xAs$, Science **327**, 665 (2010).

[44] A. Rodriguez, L. J. Vasquez, K. Slevin, and R. A. Römer, Critical Parameters from a Generalized Multifractal Analysis at the Anderson Transition, Phys. Rev. Lett. **105**, 046403 (2010).

[45] A. Rodriguez, L. J. Vasquez, K. Slevin, and R. A. Römer, Multifractal finite-size scaling and universality at the Anderson transition, Phys. Rev. B **84**, 134209 (2011).

[46] Z. M. Stadnik, D. Purdie, M. Garnier, Y. Baer, A.-P. Tsai, A. Inoue, K. Edagawa, S. Takeuchi, and K. H. J. Buschow, Electronic structure of quasicrystals studied by ultrahigh-energy-resolution photoemission spectroscopy, Phys. Rev. B **55**, 10938 (1997).

[47] E. Rotenberg, W. Theis, K. Horn, and P. Gille, Quasicrystalline valence bands in decagonal AlNiCo, Nature **406**, 602 (2000).

[48] V. A. Rogalev, O. Gröning, R. Widmer, J. H. Dil, F. Bisti, L. L. Lev, T. Schmitt, and V. N. Strocov, Fermi states and anisotropy of Brillouin zone scattering in the decagonal Al-Ni-Co quasicrystal, Nat. Commun. **6**, 8607 (2015).

[49] A. Chhabra and R. V. Jensen, Direct Determination of the f(α) Singularity Spectrum, Phys. Rev. Lett. **62**, 1327 (1989).

[50] V. K. Varma, S. Pilati, and V. E. Kravtsov, Conduction in quasiperiodic and quasirandom lattices: Fibonacci, Riemann, and Anderson models, Phys. Rev. B **94**, 214204 (2016).

[51] R. Resta and S. Sorella, Electron Localization in the Insulating State, Phys. Rev. Lett. **82**, 370 (1999).

[52] R. Resta, The insulating state of matter: A geometrical theory, Eur. Phys. J. B **79**, 121 (2011).

[53] I. Souza, T. Wilkens, and R. M. Martin, Polarization and localization in insulators: Generating function approach, Phys. Rev. B **62**, 1666 (2000).

[54] J. M. Luck and D. Petritis, Phonon spectra in one-dimensional quasicrystals, J. Stat. Phys. **42**, 289 (1986).

[55] J. Los, T. Janssen, and F. Gähler, The phonon spectrum of the octagonal tiling, Int. J. Mod. Phys. B **07**, 1505 (1993).

[56] M. Quilichini, Phonon excitations in quasicrystals, Rev. Mod. Phys. **69**, 277 (1997).

[57] M. de Boissieu, Phonons, phasons and atomic dynamics in quasicrystals, Chem. Soc. Rev. **41**, 6778 (2012).

[58] P. Brown, K. Semeniuk, D. Wang, B. Monserrat, C. J. Pickard, and F. M. Grosche, Strong coupling superconductivity in a quasiperiodic host-guest structure, Sci. Adv. **4**, eaao4793 (2018).

[59] S. Sakai, N. Takemori, A. Koga, and R. Arita, Superconductivity on a quasiperiodic lattice: Extended-to-localized crossover of Cooper pairs, Phys. Rev. B **95**, 024509 (2017).

[60] A. Ghosal, M. Randeria, and N. Trivedi, Role of Spatial Amplitude Fluctuations in Highly Disordered *s*-wave Superconductors, Phys. Rev. Lett. **81**, 3940 (1998).

[61] A. Ghosal, M. Randeria, and N. Trivedi, Inhomogeneous pairing in highly disordered *s*-wave superconductors, Phys. Rev. B **65**, 014501 (2001).

[62] V. Dobrosavljević, N. Trivedi, and J. M. Valles, Jr., *Conductor Insulator Quantum Phase Transitions* (Oxford University Press, UK, Oxford, 2012).

[63] L. C. Collins, T. G. Witte, R. Silverman, D. B. Green, and K. K. Gomes, Imaging quasiperiodic electronic states in a synthetic Penrose tiling, Nat. Commun. **8**, 15961 (2017).

[64] K. Bouadim, Y. L. Loh, M. Randeria, and N. Trivedi, Single- and two-particle energy gaps across the disorder-driven superconductor-insulator transition, Nat. Phys. **7**, 884 (2011).

[65] R. Nandkishore, J. Maciejko, D. A. Huse, and S. L. Sondhi, Superconductivity of disordered Dirac fermions, Phys. Rev. B **87**, 174511 (2013).

[66] I.-D. Potirniche, J. Maciejko, R. Nandkishore, and S. L. Sondhi, Superconductivity of disordered Dirac fermions in graphene, Phys. Rev. B **90**, 094516 (2014).

[67] J. F. Dodaro and S. A. Kivelson, Generalization of Anderson's theorem for disordered superconductors, Phys. Rev. B **98**, 174503 (2018).

[68] E. C. Andrade, E. Miranda, and V. Dobrosavljević, Electronic Griffiths Phase of the $d = 2$ Mott Transition, Phys. Rev. Lett. **102**, 206403 (2009).

[69] T. Vojta and J. A. Hoyos, Criticality and Quenched Disorder: Harris Criterion Versus Rare Regions, Phys. Rev. Lett. **112**, 075702 (2014).

[70] M. V. Feigel'man, L. B. Ioffe, V. E. Kravtsov, and E. A. Yuzbashyan, Eigenfunction Fractality and Pseudogap State Near the Superconductor-Insulator Transition, Phys. Rev. Lett. **98**, 027001 (2007).

[71] M. V. Feigel'man, L. B. Ioffe, V. E. Kravtsov, and E. Cuevas, Fractal superconductivity near localization threshold, Ann. Phys. (NY) **325**, 1390 (2010).

[72] P. W. Anderson, Theory of dirty superconductors, J. Phys. Chem. Solids **11**, 26 (1959).

[73] A. A. Abrikosov and L. P. Gor'kov, Contribution to the theory of superconducting alloys with paramagnetic impurities, J. Exptl. Theoret. Phys. (U.S.S.R.) **39**, 480 (1960) [Sov. Phys. JETP **12**, 1243 (1961)].

[74] S. N. Kempkes, M. R. Slot, S. E. Freeney, S. J. M. Zevenhuizen, D. Vanmaekelbergh, I. Swart, and C. M. Smith, Design and characterization of electrons in a fractal geometry, Nat. Phys. **15**, 127 (2019).

[75] J.-X. Zhu, K. H. Ahn, Z. Nussinov, T. Lookman, A. V. Balatsky, and A. R. Bishop, Elasticity-Driven Nanoscale Electronic Structure in Superconductors, Phys. Rev. Lett. **91**, 057004 (2003).

[76] T. Vojta, Rare region effects at classical, quantum and nonequilibrium phase transitions, J. Phys. A: Math. Gen. **39**, R143 (2006).

[77] A. Jagannathan, Quantumspins and Quasiperiodicity: A Real Space Renormalization Group Approach, Phys. Rev. Lett. **92**, 047202 (2004).

[78] K. Viebahn, M. Sbroscia, E. Carter, J. C. Yu, and U. Schneider, Matter-Wave Diffraction From a Quasicrystalline Optical Lattice, Phys. Rev. Lett. **122**, 110404 (2019).

[79] F. Flicker and J. van Wezel, One-Dimensional Quasicrystals from Incommensurate Charge Order, Phys. Rev. Lett. **115**, 236401 (2015).

[80] E. Sagi and Z. Nussinov, Emergent quasicrystals in strongly correlated systems, Phys. Rev. B **94**, 035131 (2016).

[81] A. Weiße, G. Wellein, A. Alvermann, and H. Fehske, The kernel polynomial method, Rev. Mod. Phys. **78**, 275 (2006).

[82] L. Covaci, F. M. Peeters, and M. Berciu, Efficient Numerical Approach to Inhomogeneous Superconductivity: The Chebyshev-Bogoliubov-De Gennes Method, Phys. Rev. Lett. **105**, 167006 (2010).

[83] M. Ma and P. A. Lee, Localized superconductors, Phys. Rev. B **32**, 5658 (1985).